Enhancement of Thermoelectric Performance through Transport Properties Decorrelation in the Quaternary Pseudo-Hollandite Chalcogenide Rb0.2Ba0.4Cr5Se8

Hugo Bouteiller, Bruno Fontaine, Olivier Pérez, Sylvie Hebert, Cédric Bourgès, Yoshitaka Matsushita, Takao Mori, Franck Gascoin, Jean-François Halet, David Berthebaud

Enhancement of Thermoelectric Performance Through Transport Properties Decorrelation in the Quaternary Pseudo-Hollandite Chalcogenide $Rb_{0.2}Ba_{0.4}Cr_5Se_8$

Hugo Bouteiller,[1,2] Bruno Fontaine,[3,4] Olivier Perez,[1] Sylvie Hébert,[1] Cédric Bourgès,[5] Yoshitaka Matsushita,[6] Takao Mori,[7,8] Franck Gascoin,[1] Jean-François Halet,[2,3*] and David Berthebaud[2,9*]*

[1] Laboratoire CRISMAT, ENSICAEN, UNICAEN, CNRS, Normandie Univ. (UMR 6508), Caen, France

[2] CNRS–Saint-Gobain–NIMS, IRL 3629, Laboratory for Innovative Key Materials and Structures (LINK), National Institute for Materials Science (NIMS), Tsukuba 305-0044, Japan

[3] Univ Rennes, CNRS, Ecole Nationale Supérieure de Chimie de Rennes (ENSCR), Institut des Sciences Chimiques de Rennes (ISCR), UMR 6226, F-35000 Rennes, France

[4] Saint-Cyr Coëtquidan Military Academy, CReC, F-56380 Guer, France

[5] International Center for Young Scientists (ICYS), National Institute for Materials Science, 1-1 Namiki, Tsukuba, 305-0044, Japan

[6] National Institute for Materials Science (NIMS), 1-2-1 Sengen, Tsukuba, Ibaraki 305-0047, Japan

[7] Research Center for Materials Nanoarchitectonics (MANA), National Institute for Materials Science (NIMS), 1-1 Namiki, Tsukuba 305-0044, Japan

[8] Graduate School of Pure and Applied Sciences, University of Tsukuba, Tsukuba 305-8671, Japan

[9] Nantes Université, CNRS, Institut des Matériaux de Nantes Jean Rouxel, IMN, F-44000 Nantes, France

ABSTRACT: The novel quaternary compound $Rb_{0.2}Ba_{0.4}Cr_5Se_8$ was synthesized and characterized in both single crystal and polycrystalline forms. Crystallizing in the monoclinic crystal system (space group *C*2/*m*, cell parameters a = 18.7071(4) Å, b = 3.6030(1) Å, c = 8.9637(3) Å, β = 104.494(2) °) and isostructural to pseudo-hollandite compounds, it features mixed Rb and Ba occupancy within its one-dimensional channels. High-temperature X-ray diffraction revealed no decomposition up to 973 K, and the thermal expansion coefficient at 300 K was determined to be $2.6(1)\cdot10^{-5}$ K^{-1}. Spin-polarized DFT calculations showed that the density of states for $Rb_{0.2}Ba_{0.4}Cr_5Se_8$ is more polarized than that of $Ba_{0.5}Cr_5Se_8$, resulting in a higher Seebeck coefficient, which was experimentally confirmed to reach a peak value of 400 $\mu V.K^{-1}$ at 620 K. Resistivity measurements indicated a degenerate semiconducting behavior below 550 K, with a resistivity peak of 100 mΩ.cm at that temperature, leading to a maximum power factor of 0.21 $mW.m^{-1}.K^{-2}$. Thermal conductivity measurements indicated low values around 0.8 $W.m^{-1}.K^{-1}$ in the 300 – 900 K range, resulting in a thermoelectric figure of merit of 0.22 at 873 K. Decorrelated transport properties observed in this double-inserted pseudo-hollandite compound make $Rb_{0.2}Ba_{0.4}Cr_5Se_8$ a good example of beneficial synergistic effects for higher thermoelectric performance.

INTRODUCTION

Transition metal chalcogenides (TMCs) have drawn significant attention in recent years for their remarkable transport properties stemming from their wide structural diversity.[1–5] The complex structures commonly observed in TMCs are particularly compelling in the case of thermoelectric applications.[6–8] Thermoelectric devices allow the conversion of heat into electricity and their efficiency is mostly depending on the figure of merit $zT = S^2T/\rho(\kappa_e+\kappa_L)$ of the implemented materials, S being the Seebeck coefficient, ρ the resistivity, κ_e the electric thermal conductivity, κ_L the lattice contribution to the thermal conductivity and T the absolute temperature. Highly doped degenerate semiconductors frequently exhibit remarkable thermoelectric performance, especially in compounds characterized by complex crystal structures.[9] Consequently, there is a growing interest in developing new materials with tailored structural features and appropriate transport properties to enhance thermoelectric efficiency.

The pursuit of high-performance thermoelectric materials has led the scientific community to explore various strategies.[7,9–14] One of them is to target materials having large voids or channels in their crystal structure, taking advantage of two benefits: (i) heightened phonon scattering due to the structural complexity induced by a large number of atoms per unit cell, and (ii) enhanced chemical flexibility enabling precise control of the charge carrier concentration through doping using a wide range of elements.[9] In this context, TMCs embody all the desired characteristics, and are thus the focus of this paper.

An interesting family of materials among TMCs is the pseudo-hollandite series of compounds of typical formula $A_xM_5X_8$ (A = Li, Na, K, Rb, Cs, Sr, Ba, Cd, In, Tl, Sn, and Pb; M = Sc, Ti, V, Cr; X = S, Se, Te).[15–41] Characterized by a one-dimensional channel-like structure, these compounds consist of an anionic framework constructed from edge and face-sharing MX_6

octahedra, creating spacious channels capable of accommodating an array of diverse cations. As evidenced by the large number of metals and chalcogenides stabilized in this structure type, this family of compounds offers a large playground for tuning the charge carrier concentration while maintaining low thermal conductivities due to pronounced phonon scattering. Various chemical systems within these hollandite derivatives were explored, in particular among chromium selenides. Notably, relatively high thermoelectric performance was achieved in some of them as exemplified by the zT value of 0.5 at 800 K for $Tl_xCr_5Se_8$.[24] Furthermore, it appears that deviations from the classical monoclinic $C2/m$ pseudo-hollandite structure (referred to as *A*-type) have been encountered as in $Ba_{0.5}Cr_5Se_8$ where a lowering of symmetry was observed (space group $P\bar{1}$),[15,25] and more recently with the examples of $Cs_xCr_5Te_8$ compounds exhibiting a different structural arrangement (referred to as *B*-type), favored by the presence of large cations within the channels.[42] Building on these findings, the exploration on the chromium selenide hollandite derivatives was pursued, aiming at the discovery of new structures and transport properties through the insertion of two distinct cations inside the channels. This strategy was encouraged by the facts that first, the presence of large atoms can amplify phonon scattering, potentially inducing a decrease in the lattice thermal conductivity, and on the other hand, might result in a degenerate semiconducting behavior by moving the Fermi level position, eventually leading to high thermoelectric performance. Consequently, the preparation of a chromium selenide hollandite derivative with the insertion of both barium and rubidium atoms was considered. In this study, the existence of a quaternary pseudo-hollandite compound (*A*-type) incorporating two different cations within the channels is established, and its transport properties discussed.

EXPERIMENTAL SECTION

Synthesis. $Rb_{0.2}Ba_{0.4}Cr_5Se_8$ single crystals were grown by the self-flux method in fused silica tubes from the $Rb_{0.1}Ba_{0.5}Cr_5Se_8$ nominal stoichiometry. Initially, BaSe precursor was prepared by mechanical alloying: Ba (rod, > 99 %) and Se (shots, 99.999 %) (2 x 2.5 g, balls/powder ratio 20/1, all reactants used as received from Alfa Aesar) were introduced in air in 20 mL tungsten carbide jars and loaded into a planetary ball miller (Pulverisette 7 Premium line Fritsch) at 500 rpm during 30 minutes. The high purity of BaSe was confirmed by powder X-ray diffraction. Stoichiometric amounts of BaSe, Rb_2CO_3 (powder, -20 mesh, 99%), Cr (powder, -325 mesh, 99.9%) and Se (shots, 99.999%) were loaded in fused silica tubes under Ar atmosphere, then sealed under dynamic vacuum and heated at 500 °C in 6 h. The temperature was directly raised at 900 °C in 8 h and held constant for 48 h. The samples were slowly cooled to 200 °C in 96 h and allowed to reach room temperature. The result was the formation of shiny dark needles that remain stable in ambient air. Pictures of single crystals are presented in the Supplementary Information. Powder samples of $Rb_{0.2}Ba_{0.4}Cr_5Se_8$ (10 g) were obtained by mixing the appropriate stoichiometry from the same starting reagents as for the synthesis of single crystals. The reactants were first placed in a hardened steel grinding jar (65 mL) alongside two 12.6 mm hardened-steel balls under Ar atmosphere, and subsequently ball milled during 1 h in a SPEX 8000M vibratory mixer apparatus. The obtained powder was recovered in an Ar-filled glovebox, manually ground, pelletized in a Ø 10 mm steel die and then sealed under inert atmosphere in fused silica tubes. The mixture was heated to 200 °C at 100 °C/h and held at that temperature for 4 h. The temperature was then raised to 800 °C at a heating rate of 30 °C/h and kept constant for 48 h, before being cooled to room temperature in 8 h. It should be noted that this reaction results in the generation of CO_2 gas as a by-product, leading to an increased pressure inside the sealed silica tube. However, this increase

remains limited as the stoichiometry of rubidium carbonate is very low. For instance, in a tube of 12 mm inner diameter and 12 cm length, having a free volume of about $1.36 \cdot 10^{-3}$ m^3, the resulting CO_2 pressure for the synthesis of 10 g of the title compound leads to a pressure of approx. 76 mbar, far below the atmospheric pressure. That being said, this must be kept in mind in the case of larger mass production.

Structural Characterization. Single crystals were picked up in air, isolated in silicon oil, and subsequently mounted on the goniometric head of a four-circles Rigaku XtaLAB Synergy-S diffractometer. X-ray diffraction data collection (Cu Kα (1.5418 Å) radiation) was performed on a single crystal of $Rb_{0.2}Ba_{0.4}Cr_5Se_8$. The *CrysAlisPro* software[43] was employed for crystal shape determination and the data reduction. Absorption corrections based on the crystal morphology were successfully applied. Only reflections with $I > 3\sigma(I)$ were used for the subsequent charge-flipping structure resolution from *SUPERFLIP*[44] as well as the following refinement performed with *Jana2006* software.[45] All parameters were refined with an instability factor of 0.025. Atomic displacement parameters (ADP) were systematically anisotropically refined. Rb and Ba atoms in $Rb_{0.2}Ba_{0.4}Cr_5Se_8$ evidenced a partial occupation of the 2*a* crystallographic site, their ADPs thus being fixed as equal and their occupation forced to be complementary with a partial occupation of the site equal to 0.6 (see the "**Crystal Structure Resolution**" section for more details). The powder X-ray diffraction pattern of the densified sample was measured by a Rigaku Smart Lab 3 diffractometer (Cu radiation, $\lambda_{K\alpha1}$ = 1.5418 Å, and $\lambda_{K\alpha2}$ = 1.5444 Å, $\lambda_{K\alpha2/\lambda K\alpha1}$ ratio of 0.5) with a step size of 0.02° and a scan speed of 2 °.min^{-1}. The structural model was refined using the *FULLPROF* suite[46] with the Le Bail method, yielding agreement values of R_p = 7.6 %, R_{wp} = 11.1 % and χ^2 = 1.63 (11 refined parameters). High-temperature powder X-ray diffraction (HT-XRD) patterns were carried out on the post-synthesis powder up to 973 K, using a Rigaku SmartLab 9

kW (monochromatic Cu radiation, $\lambda_{K\alpha 1}$ = 1.54056 Å) under dry N_2 gas flow (1 L.min^{-1}) with a step width of 0.02 ° and a scan speed of 1 °.min^{-1}. The heating and cooling rates were 5 °C.min^{-1} each, and the temperature was held constant for 5 minutes before each measurement.

Physical Properties Characterization. Powders of the aforementioned compound were densified in 10 mm diameter graphite dies using an SPS DrSinter apparatus with a run under vacuum at 800 °C for 10 min (heating/cooling rates of 80 °C/min), and applying a pressure of 50 MPa before heating. The density of the obtained pellet measured by the Archimedes' method was 5.406 g.cm^{-3}, resulting in a relative density of 98.9 %. Seebeck coefficient and resistivity were measured simultaneously using a ZEM5 apparatus (ULVAC) on a 3 x 3 x 10 mm shaped bar. The charge carrier concentration was measured at room temperature by a Physical Property Measurement System (PPMS) using the Hall configuration under a magnetic field ranging from −9 to 9 T. Thermal conductivity was characterized by a NETZSCH 467 HyperFlash laser-flash apparatus on 10-mm diameter and 2-mm thickness pellets, coated with graphite. The heat capacity was estimated using the Dulong-Petit law. Uncertainties on the Seebeck coefficient, resistivity, power factor and figure of merit zT are 6 %, 8 %, 14% and 20 %, respectively.

Electronic Structure Calculations. Periodic spin-polarized density functional theory (DFT) calculations were carried out to provide insights into the electrical structural properties of the title compound. Structural optimizations were first performed using the *VASP* software version 5.4.1 [47–49] with the Perdew, Burke and Ernzerhof (PBE) exchange-correlation functional[50] and a cut-off energy of 350 eV. The non-stoichiometric unit cells of $Ba_{0.5}Cr_5Se_8$ and $Rb_{0.2}Ba_{0.4}Cr_5Se_8$ were obtained from a 2 x 1 x 1 supercell (27 atoms in total) and a 1 x 5 x 1 supercell (136 atoms in total), respectively, that were sampled with a 6 x 6 x 6 Monkhorst-Pack *k*-points grid.[51] *VASP*-relaxed structures were then used to compute the electronic density of states (DOS) with the

WIEN2k code using the full-potential linearized augmented plane wave approach,[52] employing the modified Becke-Johnson (mBJ) exchange-correlation potential[53] with a plane-wave cut-off corresponding to $R_{MT} \cdot K_{max} = 7$. Total energy convergence was achieved with a Brillouin Zone (BZ) integration mesh of 500 *k*-points. Electronic transport coefficients were calculated within the linearized Boltzmann transport equation using the *BoltzTrap2* code[54] with a constant relaxation time for the electrons and assuming a rigid band structure[55,56] with respect to the Fermi energy. 5000 *k*-points in the BZ were used to compute the band derivatives for transport calculations. The Seebeck coefficient (S) as function of the chemical potential (μ) that indicates the doping level or carrier concentration in the considered system, was calculated at 300 and 800 K. Positive and negative values of μ indicate *n*-type and *p*-type doping, respectively.

RESULTS AND DISCUSSION

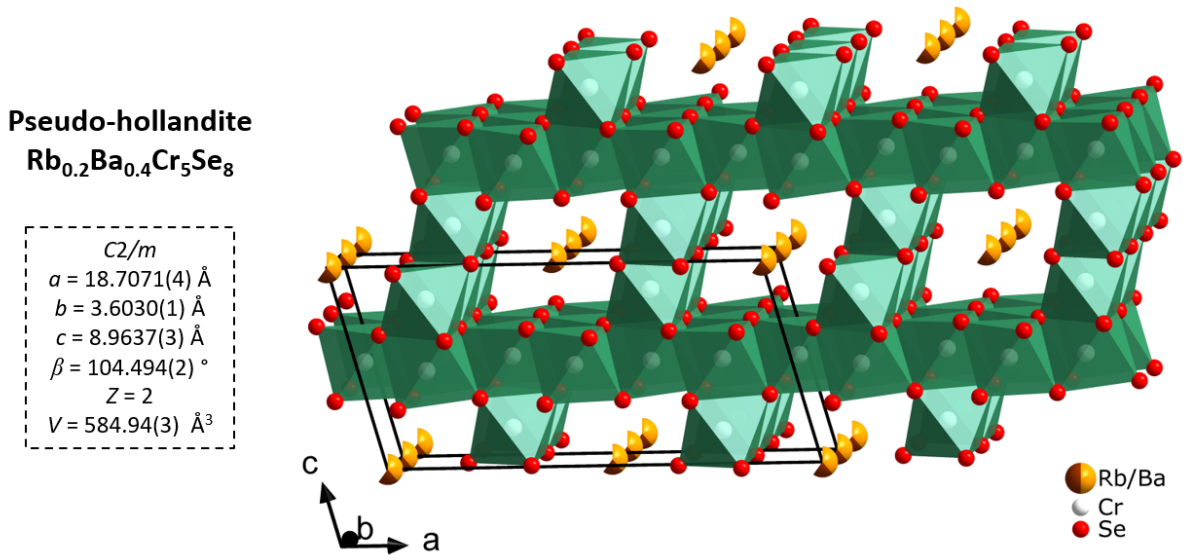

Figure 1. Structural arrangement of the $Rb_{0.2}Ba_{0.4}Cr_5Se_8$ pseudo-hollandite compound (*A*-type). The partial occupancies of both Rb (brown) and Ba (orange) cations within the channels are represented by fragmented spheres.

Crystal Structure Solution and Refinement. $Rb_{0.2}Ba_{0.4}Cr_5Se_8$ crystallizes in the pseudo-hollandite *A*-type structure, as commonly encountered for the $A_xM_5Se_8$ reported structures (A = alkali/alkaline-earth, M = transition metal), with a mixed occupancy of Rb and Ba atoms on the 2*a* site inside the channels (**Figure 1**). Examination of single-crystal X-ray diffraction frames unveiled the monoclinic symmetry, which interestingly differs from that of $Ba_{0.5}Cr_5Se_8$ exhibiting triclinic symmetry (space group $P\bar{1}$).[15] This difference led to further investigation on the possibility of either exclusive Rb insertion, supported by the existence of $RbCr_5Se_8$,[17,30,31] or simultaneous insertion of both Rb and Ba. Data reduction was made in the monoclinic symmetry, using a numerical absorption correction with spherical harmonics model, and the space group was confirmed to be *C*2/*m*.

The initial structure solution obtained from *Superflip* yielded the expected anionic framework built of $CrSe_6$ octahedra, and the so-formed channels were filled with Rb atoms respective to the $RbCr_5Se_8$ stoichiometry at first to evaluate the possibility of being in the presence of this latter compound. Atomic positions and anisotropic ADPs were refined with an instability factor of 0.025, resulting in a refined model with a *R* value of 3.94 % and GOF = 3.28. Rb occupation in the channels was then refined, yielding at this point the $Rb_{0.809}Cr_5Se_8$ composition with *R* = 2.65 % and GOF = 1.71. However, this model exhibited significant electronic residues in Fourier difference maps, thus appeared unacceptable. Additionally, complementary energy dispersive X-ray spectroscopy (EDS) experiments on multiple single crystals confirmed the presence of both Rb and Ba cations. Consequently, the splitting of the Rb atom site involving a partial Rb/Ba occupation was considered. The nominal composition being $Rb_{0.1}Ba_{0.5}Cr_5Se_8$, 60 % of the crystallographic site (2*a*) is expected to be occupied by cations, therefore the total occupancy of both Rb and Ba atoms were fixed accordingly. Ba relative occupancy was adjusted such that Rb

and Ba atoms occupy 10 % and 50 % of the cationic site, respectively, consistent with the $Rb_{0.1}Ba_{0.5}Cr_5Se_8$ nominal composition. ADPs and atomic positions of the cationic atoms were constrained to be equal. Subsequent refinement led to an improved model with an *R* value of 2.43 % and GOF = 1.44. Occupancies of the cationic atoms were then refined and a final refinement process including extinction correction granted the title compound $Rb_{0.213(5)}Ba_{0.387(5)}Cr_5Se_8$, agreement values dropping to *R* = 1.72 % and GOF = 1.05. Examination of Fourier difference maps confirmed minimal electronic residues (< 0.66 $e^-.Å^{-3}$), validating the accuracy of this structural model. Counting the charges, both Rb and Ba contributions lead to a total of 0.987 electrons conceded to the Cr_5Se_8 anionic framework, closely approaching the expected value of one electron for this polar chromium selenide as in $Ba_{0.5}Cr_5Se_8$. Detailed crystallographic data, including structure resolution details, are provided in **Table 1**. Refined coordinates and ADPs are displayed in **Table 2** and the main interatomic distances are summarized in **Table 3**.

Table 1. Crystallographic Data of $Rb_{0.2}Ba_{0.4}Cr_5Se_8$ from the Single-crystal X-ray Diffraction Study

Formula	$Rb_{0.2}Ba_{0.4}Cr_5Se_8$
Structural type	*A* (pseudo-hollandite)
Molar mass ($g.mol^{-1}$)	963.68
Crystal system	Monoclinic
Space group	*C*2/*m* (12)
a (Å)	18.7071(4)
b (Å)	3.6030(1)
c (Å)	8.9637(3)
β (°)	104.494(2)
V ($Å^3$)	584.94(3)
Z	2
Calculated density ($g.cm^{-3}$)	5.4676
Data collection	
T (K)	293
Crystal description	Black needle
Crystal dimensions (mm^3)	0.016 x 0.014 x 0.163

Radiation	Cu (1.54184 Å)
$\mu_{(Cu\ K\alpha)}$ (mm^{-1})	76.137
2θ limits (°)	4.86 – 75.48
hkl range	$-22 < h < 22$ $-3 < k < 4$ $-11 < l < 11$
Measured reflections	5486
Data reduction	
Independent reflections	718
Independent reflections with $I > 3\sigma(I)$	704
R_{int}	0.0221
Transmission factors	0.155 – 1
Refinement	
R_F^2 (obs/all)	0.0172/0.0281
R_{WP} (obs/all)	0.0176/0.0289
Goodness of fit	1.05
Refined parameters	47
$\Delta\rho_{min}/\Delta\rho_{max}$ ($e^-.Å^{-3}$)	–0.66/0.53

Crystal Structure Discussion. The existence of the double inserted $Rb_{0.2}Ba_{0.4}Cr_5Se_8$ crystallizing in the classical pseudo hollandite structure reveals that the presence of a large cation such as Rb (atomic radius = 2.35 Å) in the channel stabilizes this structure-type. Indeed, $Ba_{0.5}Cr_5Se_8$ exhibits a lowering of symmetry towards the triclinic space group $P\bar{1}$ which results from a distortion of the arrangement of $CrSe_6$ octahedra in the anionic framework.[15] As a consequence, the distortion of the anionic framework is reduced when both Rb and Ba are inserted, this behavior being explained by the presence of Rb atoms which, even in a limited amount, stabilizes the classical pseudo-hollandite structure type (*A*-type). Such an effect has already been encountered, as the presence of large cation like Rb (atomic radius = 2.35 Å) or Cs (atomic radius = 2.60 Å) in the channels were proved to modify the structure from the *A*-type pseudo-hollandite to the *B*-type hollandite-like compounds, in which the arrangement of the channels differs.[18,19,42] Notably, the range of compositions for a given structural type can be narrow, exemplified by $Rb_{0.62}Cr_5Te_8$ and

$Rb_{0.73}Cr_5Te_8$ which are of *A*-type and *B*-type, respectively.[19,20] Furthermore, it can be noted that the title compound finds a notable stability with the $Rb_{0.2}Ba_{0.4}Cr_5Se_8$ particular composition, involving a site occupancy of 60 % on the cation site (2*a*). This includes a Ba amount approximately twice as large as that of Rb, indicating that other intermediate compositions, away from classical $(A^{2+})_{0.5}Cr_5Se_8$ or $A'Cr_5Se_8$ (A = alkaline earth; A' = alkaline), can be obtained within this family of compounds. This opens up further possibilities when considering adjusting the charge carrier concentration and doping level in such compounds.

The cell parameters of the title compound (a = 18.7071(4) Å, b = 3.6030(1) Å, c = 8.9637(3) Å, β = 104.494(2) °) closely aligns with those of other pseudo-hollandite compounds such as $Tl_xCr_5Se_8$,[24] KCr_5Se_8,[17] or $NaCr_5Se_8$.[17] They are however slightly smaller than those of $RbCr_5Se_8$ and $CsCr_5Se_8$.[17,30,31] This may be explained by both a higher amount and a larger atomic radius of the inserted cations in these two compounds. A large anisotropic atomic displacement parameter is observed along the channel direction (*b*-axis) as reflected by extended values of U_{22} = 0.08 Å^2, manifold larger than those in other directions (**Table 2**). This phenomenon is recurrent in several pseudo-hollandite compounds, particularly in the cases of partially-filled compounds such as $Tl_xCr_5Se_8$,[24] $Tl_xV_5S_8$,[34] $A_xCr_5Se_8$ (A = Rb, Cs)[22] or *B*-type $A'_xCr_5Te_8$.(A' = Rb, Cs).[19,42] It can be attributed to the relatively low geometrical restrictions of these cations along the *b*-axis (channel axis) compared to other directions, due to the presence of the channel walls. In addition, it can be further accentuated by the presence of vacancies of the 2*a* cationic site as 40 % of the site remains unoccupied, resulting in a potential cationic disorder.

The Cr–Se bond lengths range from 2.4814(4) to 2.6211(4) Å, consistent with those observed in other chromium selenide pseudo-hollandites (**Table 3**). Notably, the principal short Cr–Cr distance in the title compound (Cr(2)–Cr(3) = 3.0631(7) Å) is slightly longer than that in $RbCr_5Se_8$

(3.0568(4) Å) and $CsCr_5Se_8$ (3.0480(4) Å).[30] This trend aligns with the increasing size of the inserted cations in the ACr_5Se_8 (*A* = Rb/Ba, Rb, Cs) series, resulting in a larger intercationic distance in the channels (Rb/Ba–Rb/Ba = 3.6030(1) Å, Rb–Rb = 3.623(1) Å, Cs–Cs = 3.637(1) Å), and a more constricted anionic framework in the pseudo-hollandites inserted with large-radius cations.

Table 2. Refined Coordinates and Atomic Displacement Parameters for $Rb_{0.2}Ba_{0.4}Cr_5Se_8$ (Estimated Standard Deviations are Given in Brackets).

Atom	Wyckoff position	SOF	*x*	*y*	*z*	U_{iso}	U_{11} (Å^2)	U_{22} (Å^2)	U_{33} (Å^2)	U_{13} (Å^2)
Rb	2*a*	0.213(5)	0	0	0	0.0426(3)	0.0268(4)	0.0800(7)	0.0179(4)	0.0000(3)
Ba	2*a*	0.387(5)	0	0	0	0.0426(3)	0.0268(4)	0.0800(7)	0.0179(4)	0.0000(3)
Cr1	2*d*	1	0	½	½	0.0096(2)	0.0095(3)	0.0078(4)	0.0110(4)	0.0014(3)
Cr2	4*i*	1	0.8427(1)	0	0.5174(1)	0.0096(2)	0.0089(3)	0.0080(3)	0.0118(3)	0.0026(2)
Cr3	4*i*	1	0.7951(1)	0	0.1647(1)	0.0092(2)	0.0091(3)	0.0078(3)	0.0100(3)	0.0012(2)
Se1	4*i*	1	0.9262(1)	0	0.3382(1)	0.0098(2)	0.0085(2)	0.0078(2)	0.0121(2)	0.0006 (2)
Se2	4*i*	1	0.9145(1)	½	0.6783(1)	0.0108(1)	0.0103(2)	0.0090(2)	0.0128(2)	0.0022(2)
Se3	4*i*	1	0.6682(1)	0	-0.0061(1)	0.0103(2)	0.0110(2)	0.0086(2)	0.0108(2)	0.0017 (2)
Se4	4*i*	1	0.7396(1)	0	0.6576(1)	0.0093(2)	0.0095(2)	0.0070(2)	0.0117(2)	0.0032(2)

Table 3. Interatomic Distances (Å) in $Rb_{0.2}Ba_{0.4}Cr_5Se_8$ (Estimated Standard Deviations are Given in Brackets).

$CrSe_2$ layer (ab plane)	Cr1–Se1	2.5004(2) x 4	Bridging Cr–Se octahedra	Cr3–Se1	2.5547(4)	A–Se	Rb/Ba–Se1	3.6322(3) x 2
	Cr1–Se2	2.5279(4) x 2		Cr3–Se3	2.4819(4)		Rb/Ba–Se2	3.4369(3) x 4
	Cr2–Se1	2.5050(7)		Cr3–Se3	2.4952(4) x 2		Rb/Ba–Se3	3.6379(3) x 4
	Cr2–Se2	2.4814(4) x 2		Cr3–Se4	2.5931(4) x 2			
	Cr2–Se4	2.5513(7)						
	Cr2–Se4	2.6211(4) x 2						
Principal short Se–Se	Se1–Se1	3.4678(3)	Principal short Cr–Cr	Cr2–Cr3	3.0631(7)	Principal short A–A	A–A (A = Rb, Ba)	3.6030(1)
	Se4–Se4	3.4532(4)						

Bulk $Rb_{0.2}Ba_{0.4}Cr_5Se_8$ investigation. A pure powdered sample of the title compound was synthesized and densified by spark plasma sintering (SPS). The powder X-ray diffraction pattern and refined structural model are displayed in **Figure 2**. Results suggest the presence of a single phase with the cell parameters a = 18.7128(4) Å, b = 3.6024(2) Å, c = 8.9604(2) Å and β = 104.522(1) °, comparing well with those obtained from the single-crystal X-ray diffraction study.

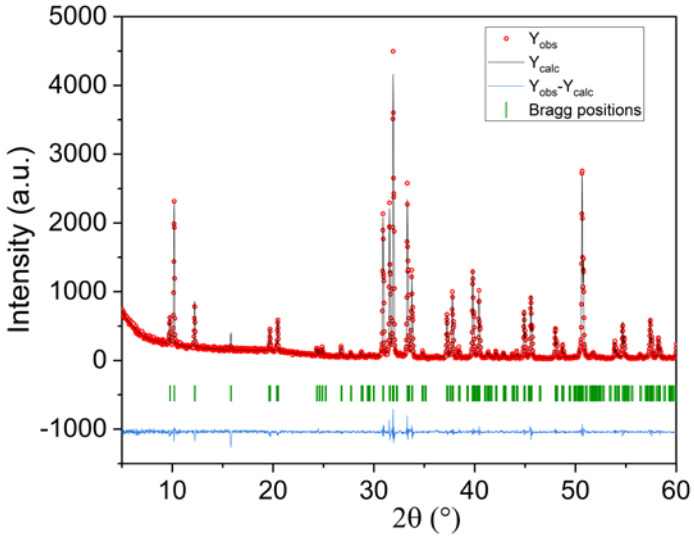

Figure 2. Powder X-ray diffraction pattern of a densified $Rb_{0.2}Ba_{0.4}Cr_5Se_8$ sample, refined with the Le Bail method. The experimental data are plotted in red dots, the refined model in black, the difference curve in blue and the Bragg reflections are displayed in green bars.

HT-XRD patterns were measured to assess the thermal stability of the title compound, in particular possible degradation or decomposition into secondary phases with rising temperature. The results are sketched in **Figure 3**. Up to 973 K under inert atmosphere (N_2), $Rb_{0.2}Ba_{0.4}Cr_5Se_8$ exhibits no particular degradation or decomposition, as no secondary phases were detected with increasing temperature. Subsequent Le Bail refinements of the structural models matching recorded patterns were carried out and provided the evolution of the unit cell volume of the title compound with temperature variation (**Figure 4**). The thermal expansion coefficient of $Rb_{0.2}Ba_{0.4}Cr_5Se_8$ was consequently determined to be $2.6(1).10^{-5}$ K^{-1} at 300 K. This value is of high interest as the thermal

expansion of thermoelectric materials is a critical parameter in the implementation of a given material in thermoelectric devices.[57]

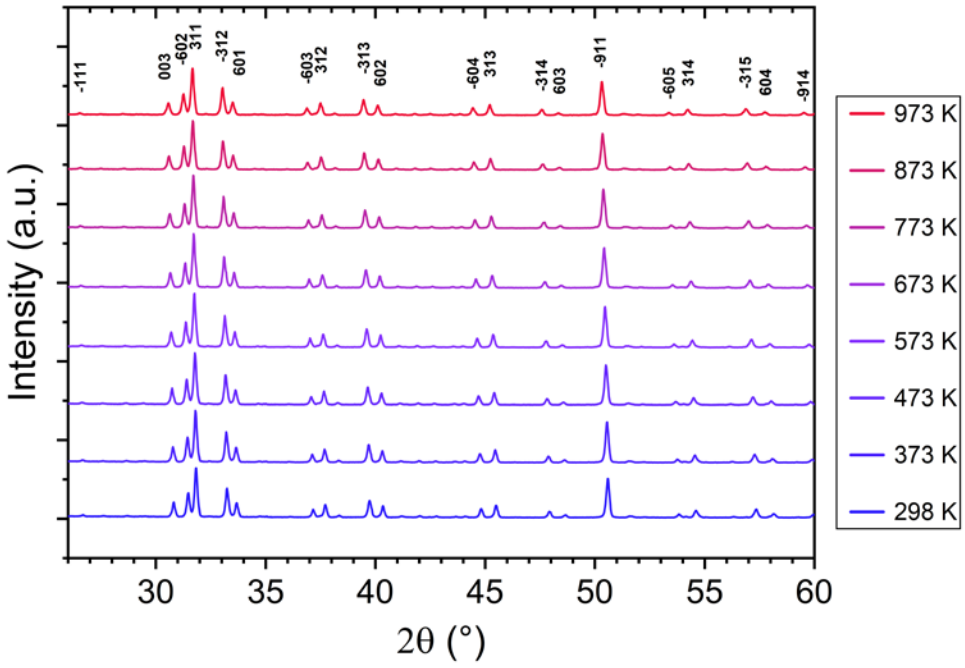

Figure 3. HT-XRD patterns showing the thermal stability of the crystal structure of $Rb_{0.2}Ba_{0.4}Cr_5Se_8$ with temperature up to 973 K.

An electron dispersive X-ray spectroscopy analysis was carried out on the densified sample (**Figure 5**), revealing a good chemical homogeneity with the presence of all elements of the quaternary

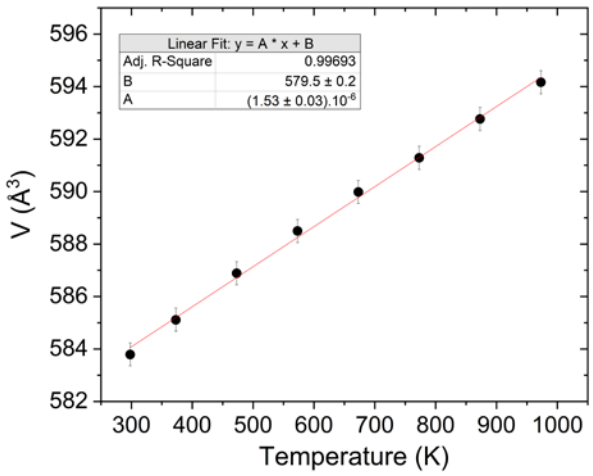

Figure 4 - Volume of the unit cell as a function of temperature, allowing the determination of the linear thermal expansion coefficient $(2.6(1).10^{-5}\ K^{-1}$ at 300 K)

compound. Quantitative analyses performed on three different zones of the sample resulted in the averaged chemical composition $Rb_{0.19(2)}Ba_{0.34(2)}Cr_{4.95(12)}Se_8$, closely aligning with the composition of the title compound. Traces of CrO_2 could locally be detected, most probably resulting from the carbonate starting reactant, but remain marginal as no evidence of a CrO_2 phase could be detected with respect to powder X-ray diffraction. Additional EDS characterizations are presented in the Supplementary Information.

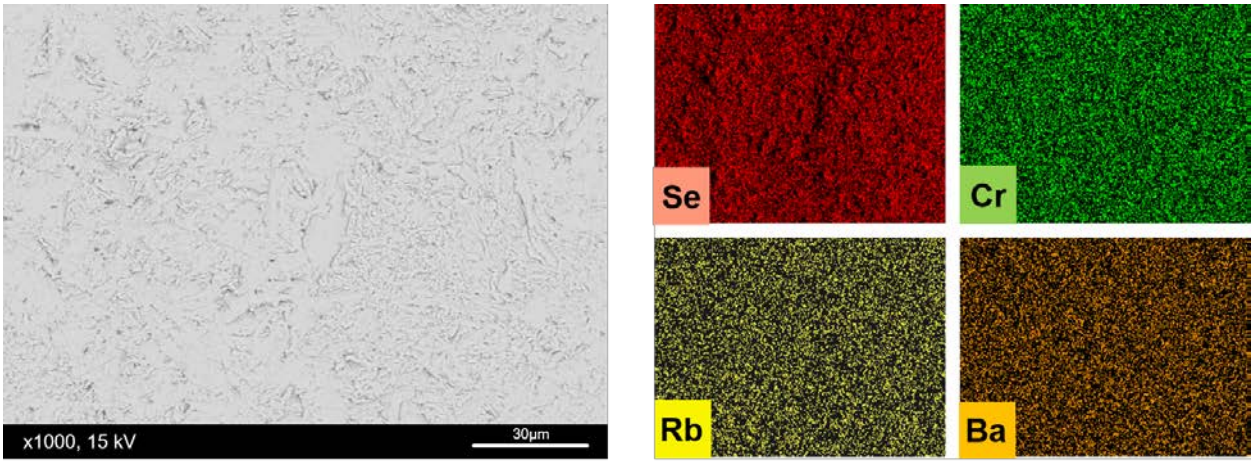

Figure 5. Energy Dispersive X-ray Spectroscopy (EDS) of a densified sample of $Rb_{0.2}Ba_{0.4}Cr_5Se_8$. The measured samples exhibited a chemical composition of $Rb_{0.19(2)}Ba_{0.34(2)}Cr_{4.95(12)}Se_8$, matching that of both nominal composition and single-crystal X-ray diffraction experiments.

Theoretical Investigation. Density functional theory calculations were carried out to obtain insights on the expected electronic and transport properties of $Rb_{0.2}Ba_{0.4}Cr_5Se_8$ (see the Experimental Section for the computational details). Its density of states (DOS) is shown in **Figure 6** and compared to that of isoelectronic $Ba_{0.5}Cr_5Se_8$. In both cases, the DOS around the Fermi level is predominantly Cr and Se in character with hardly any participation of the cations. If we assume a complete charge transfer from the inserted cation to the chromium-selenium framework ($(Rb_{0.2})^{+}(Ba_{0.4})^{2+}[Cr_5Se_8]^{-}$ and $(Ba_{0.5})^{2+}[Cr_5Se_8]^{-}$), a semiconducting behavior is expected for both compounds – which was well characterized experimentally for $Ba_{0.5}Cr_5Se_8$.[15,25] Indeed, this is confirmed computationally with a favorable band gap of *ca*. 0.5 eV for $Rb_{0.2}Ba_{0.4}Cr_5Se_8$ and *ca*. 1

eV for $Ba_{0.5}Cr_5Se_8$. With a smaller band gap, we expect that the resistivity of the former compound should be lower than that of the latter one. Another interesting point is that the spin-up and spin-down total and Cr-projected DOS strongly differ, demonstrating a firmly polarized DOS compared to that of $Ba_{0.5}Cr_5Se_8$ which shows no particular spin-related difference (see **Figure 6**). The computed DOS near the Fermi level suggests the presence of multiple bands with a small band-gap which could in turn lead to a significant contribution of minority carriers in the electrical conduction.

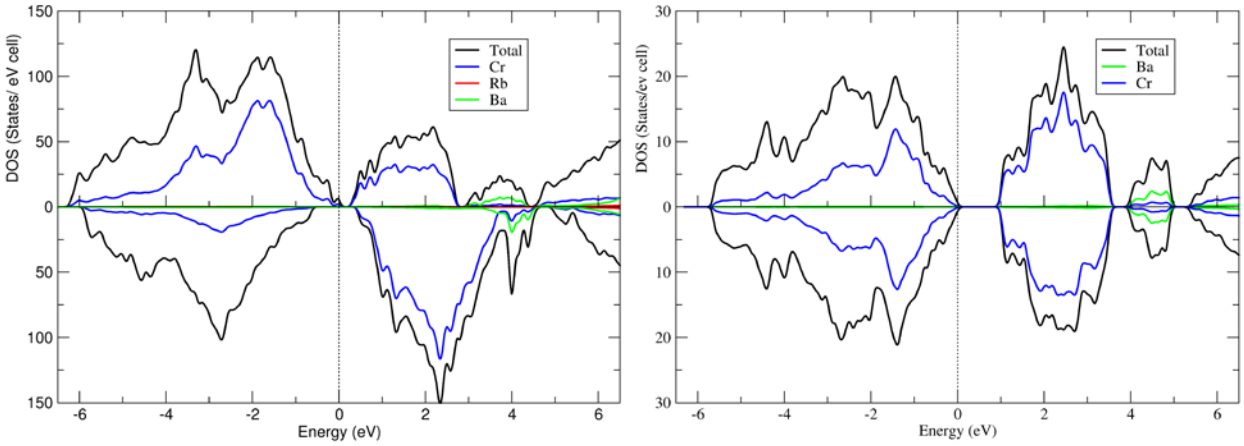

Figure 6. Spin-polarized total and atom-projected DOS of $Rb_{0.2}Ba_{0.4}Cr_5Se_8$ (left) and $Ba_{0.5}Cr_5Se_8$ (right).

The Seebeck coefficient (thermopower) as function of the chemical potential was computed for $Rb_{0.2}Ba_{0.4}Cr_5Se_8$ and $Ba_{0.5}Cr_5Se_8$ for comparison (see the Experimental Section for the computational details). As shown in **Figure 7**, it is very sensitive to the chemical potential and temperature. At both temperatures, high peak values of the Seebeck coefficient are computed for *p*-type and *n*-type doping at 300 K and 800 K in the vicinity of the Fermi level (μ = 0 eV), which indicates that fairly large values of *S* can be attained upon *p*-type or *n*-type doping. Interestingly, peak values computed for $Rb_{0.2}Ba_{0.4}Cr_5Se_8$ are higher than those computed for $Ba_{0.5}Cr_5Se_8$ (1700 vs. 1200 $\mu V.K^{-1}$ at 300 K for instance for *p*-type). This is in agreement with experiments which

show thermopower higher for the former than for the latter (*vide supra*). We note as well that the *S* curve for $Rb_{0.2}Ba_{0.4}Cr_5Se_8$ is more 'complex' than that for $Ba_{0.5}Cr_5Se_8$ due a more spin-polarized DOS for the former.

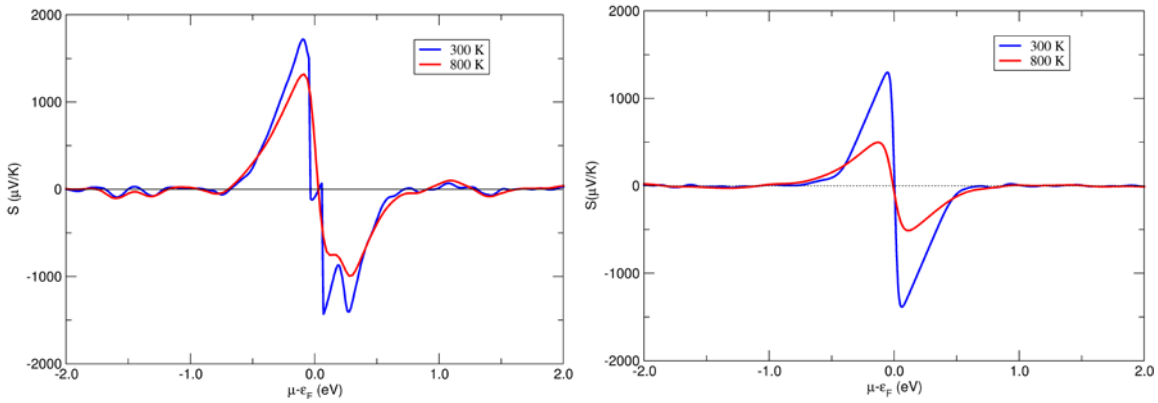

Figure 7. Seebeck coefficient (*S*) as a function of the chemical potential (μ) computed for $Rb_{0.2}Ba_{0.4}Cr_5Se_8$ (left) and $Ba_{0.5}Cr_5Se_8$ (right), at 300 K (blue line) and 800 K (red line).

Transport Properties. Transport properties of $Rb_{0.2}Ba_{0.4}Cr_5Se_8$ were measured on a densified sample. The Seebeck coefficient, electrical resistivity and resulting power factor are displayed in **Figure 8**, including those of other pertinent pseudo-hollandites for comparison. The Seebeck coefficient of $Rb_{0.2}Ba_{0.4}Cr_5Se_8$ remains positive across the entire temperature range, indicating that holes are the dominant charge carriers in this compound. Thermopower values increase with temperature until reaching a peak value of about 400 $\mu V.K^{-1}$ at 620 K, followed by a decrease at higher temperatures, attributed to the thermal activation of minority carriers. The Seebeck coefficient evolution with temperature is similar to that of $Ba_{0.5}Cr_5Se_8$, with the notable distinction that the absolute values for $Rb_{0.2}Ba_{0.4}Cr_5Se_8$ are substantially higher throughout the temperature range, an advantageous characteristic regarding thermoelectric performance. The charge carrier concentration (*p*) was measured to be 1.7×10^{19} cm^{-3} at 300 K. This value is slightly lower than that of $Tl_xCr_5Se_8$ (4.5×10^{19} cm^{-3} at 300 K) for instance,[24] which is consistent with the increased

Seebeck coefficient observed in $Rb_{0.2}Ba_{0.4}Cr_5Se_8$. It is however significantly higher than the value measured for $Ba_{0.5}Cr_5Se_8$ (4.4 x 10^{18} cm^{-3}),[15] in good agreement with the intrinsic semiconducting behavior observed in the latter compound.

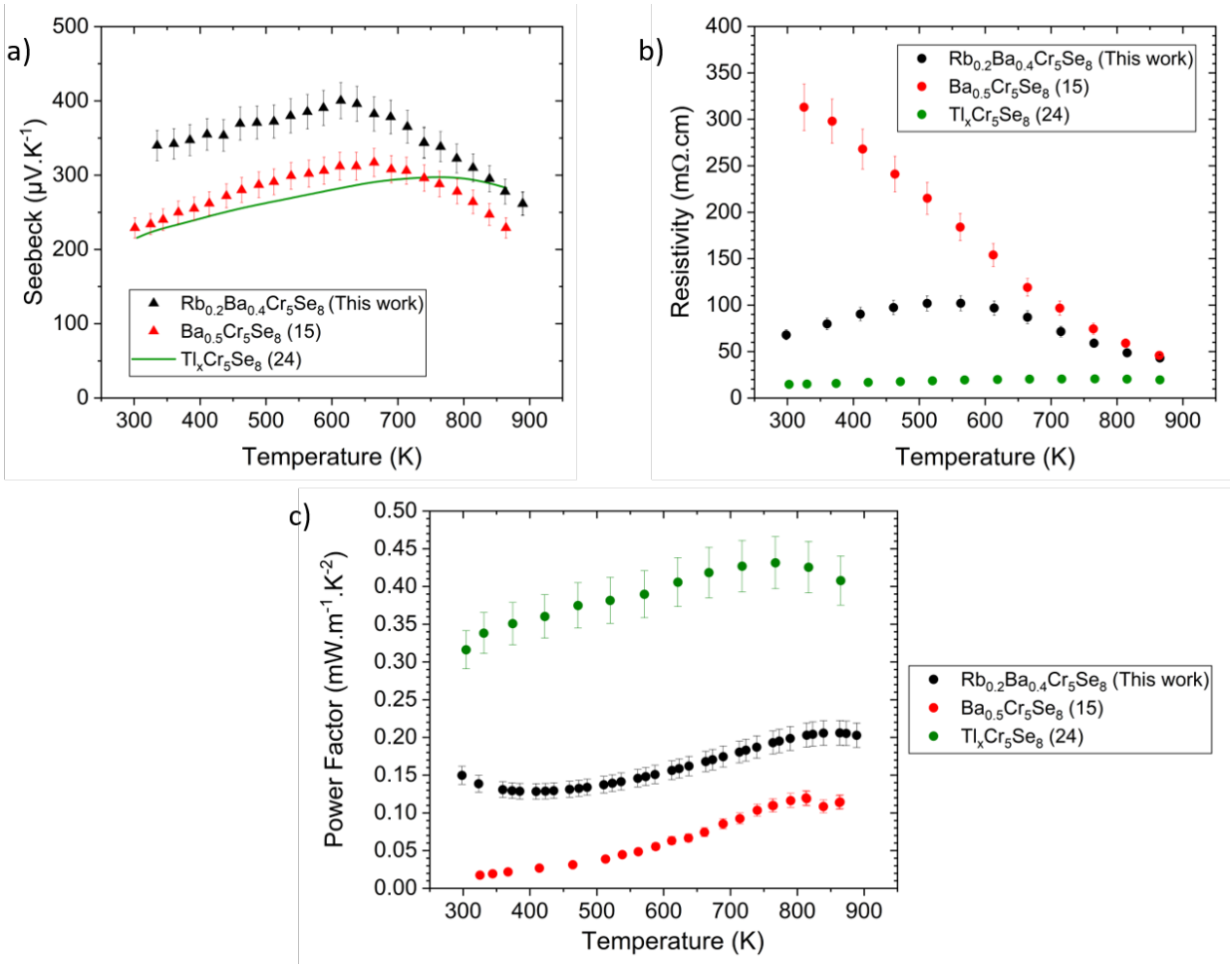

Figure 8. Transport properties of $Rb_{0.2}Ba_{0.4}Cr_5Se_8$ and comparison with $Ba_{0.5}Cr_5Se_8$ and $Tl_xCr_5Se_8$ pseudo-hollandites. a) Seebeck coefficient, b) Resistivity and c) Power Factor.

The resistivity of $Rb_{0.2}Ba_{0.4}Cr_5Se_8$ is displayed in **Figure 8b**. It is measured to be about 65 mΩ.cm at room temperature, then increases with temperature to a maximum value of 100 mΩ.cm at 550 K before decreasing with further temperature elevation, revealing a transition from a degenerate semiconductor conduction mode to a non-degenerate conductive behavior above 550 K. $Rb_{0.2}Ba_{0.4}Cr_5Se_8$ exhibits a distinct conductive behavior compared to $Ba_{0.5}Cr_5Se_8$, which presents a semiconducting behavior on the entire temperature range.[15,25] This discrepancy is

attributed to a slightly different Fermi level position, expected to reside in the band gap for $Ba_{0.5}Cr_5Se_8$. It thus appears that the somewhat complex band structure of $Rb_{0.2}Ba_{0.4}Cr_5Se_8$ near the Fermi level induces the latter to lie inside the valence band, near the band edge, resulting in a degenerate semiconductor behavior below 550 K for this compound. When temperature rises up, the dispersion of the bands causes the Fermi level to shift away from the valence band, ending up in the bandgap and thus inducing a semiconducting behavior, as observed in Cu_2SnSe_3 for instance.[58] As often observed for small band-gap semiconductors,[59] the thermal activation of minority carriers above 550 K might also trigger hole-electron recombination and induce bipolar conduction, resulting in an increase of carrier concentration and a decrease of the Seebeck coefficient with temperature which is consistently observed experimentally.

Furthermore, the electrical conduction behavior of $Rb_{0.2}Ba_{0.4}Cr_5Se_8$ present similarities with that of $Tl_xCr_5Se_8$, as the latter was reported to exhibit a metallic conductive behavior due to Tl deficiency in the temperature range of 200 – 750 K.[24] This observation supports the fact that the Fermi level reside deeper in the valence band in $Tl_xCr_5Se_8$ compared to $Rb_{0.2}Ba_{0.4}Cr_5Se_8$, resulting in an increased hole concentration, enhanced mobility, and subsequently lower resistivity in $Tl_xCr_5Se_8$.[24] $Rb_{0.2}Ba_{0.4}Cr_5Se_8$ thus stands as an intermediate case between a semiconductor ($Ba_{0.5}Cr_5Se_8$) and a highly degenerated semiconductor ($Tl_xCr_5Se_8$).

Remarkably, a clear decorrelation of the electrical transport properties can be observed in $Rb_{0.2}Ba_{0.4}Cr_5Se_8$, especially when compared to $Ba_{0.5}Cr_5Se_8$. A first decorrelation of the Seebeck coefficient and the resistivity was observed in the solid solution $Ba_{0.5+x}Cr_5Se_8$ ($0 < x < 0.05$). Indeed, the excess of Ba in the $Ba_{0.5+x}Cr_5Se_8$ solid solution led to a decrease in the Seebeck coefficient and an increased resistivity.[25] In the case of $Rb_{0.2}Ba_{0.4}Cr_5Se_8$, the opposite decorrelation is found, as the Seebeck coefficient is observed to increase while the resistivity decreases when

compared to $Ba_{0.5}Cr_5Se_8$. This decorrelation might be explained by the evolution of the density of states effective mass resulting from a slight variation of the band structure near the Fermi level. In particular, the hole effective mass m^* was calculated and compared for both $Ba_{0.5}Cr_5Se_8$ and $Rb_{0.2}Ba_{0.4}Cr_5Se_8$ in the parabolic band structure approximation at 300 K, yielding values of about 0.3 m_0 and 1.1 m_0, respectively. These absolute values must be taken with great care, however allow comparison between both compounds, as the higher effective mass of $Rb_{0.2}Ba_{0.4}Cr_5Se_8$ can be well explained by its degenerate semiconducting behavior at 300 K. Such a situation was also encountered in other several chalcogenides, including isostructural $Tl_xCr_5Se_8$,[24] or the copper selenides Cu_2SnSe_3 and Cu_3SbSe_4 for instance, where a partially degenerate conductive behavior was observed as well.[58,60,61] The synergistic increase of the Seebeck coefficient and decrease of resistivity in $Rb_{0.2}Ba_{0.4}Cr_5Se_8$ is beneficial for the thermoelectric properties optimization, as it leads to an enhanced maximum power factor of 0.20 $mW.m^{-1}.K^{-2}$ at 850 K, substantially higher than that of $Ba_{0.5}Cr_5Se_8$ (0.12 $mW.m^{-1}.K^{-2}$ at 830 K, see **Figure 8c**). The mobility of the charge carriers (μ) was calculated to be 5.5 $cm^2.V^{-1}.s^{-1}$ at room temperature, slightly higher than the value reported for $Ba_{0.5}Cr_5Se_8$ which is below 5 $cm^2.V^{-1}.s^{-1}$,[25] but about half that of $Tl_xCr_5Se_8$ (10 $cm^2.V^{-1}.s^{-1}$).[24] This explains why the power factor still remains higher for the latter compound in the studied temperature range.

The thermal conductivity of the title compound exhibits a gradual decrease with temperature from room temperature to a minimum value of about 0.8 $W.m^{-1}.K^{-1}$ at 773 K (**Figure 9a**). Both $Rb_{0.2}Ba_{0.4}Cr_5Se_8$ and $Ba_{0.5}Cr_5Se_8$ exhibit a similar thermal conductivity behavior, with the former exhibiting slightly lower values while still falling within the standard deviation range with respect to the latter. However, this subtle decrease may stem from a heightened phonon scattering mechanism in $Rb_{0.2}Ba_{0.4}Cr_5Se_8$, due to the high atomic mass fluctuation inside the channels in the

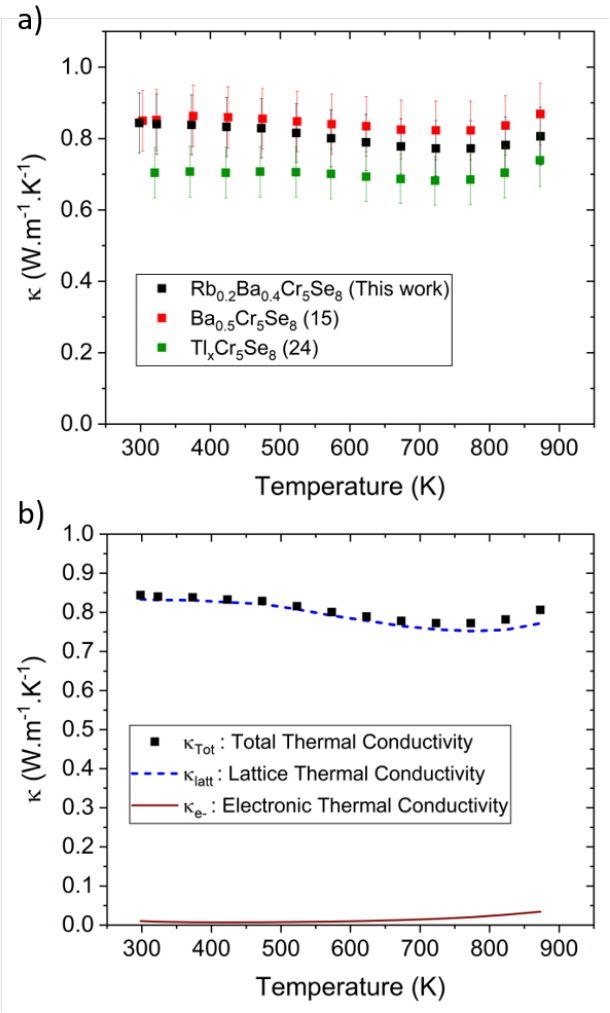

Figure 9 – a) Total thermal conductivity of $Rb_{0.2}Ba_{0.4}Cr_5Se_8$, and comparison to other pseudo-hollandites ($Ba_{0.5}Cr_5Se_8$ and $Tl_xCr_5Se_8$). b) Electronic and lattice contributions to the thermal conductivity of $Rb_{0.2}Ba_{0.4}Cr_5Se_8$.

double-inserted pseudo-hollandite. A slight increase is also observed from 750 K upwards, consistent with the thermal activation of minority carriers contributing to the electrical thermal conductivity component (**Figure 9b)**. Nevertheless, the total thermal conductivity remains largely dominated by the lattice thermal part which maintains low values (between 0.75 and 0.82 $W.m^{-1}.K^{-1}$). Notably, it can be observed that $Tl_xCr_5Se_8$ exhibits lower thermal conductivity values, primarily caused by a heavier element (Tl) in the channel than Rb or Ba, inducing a stronger local mass fluctuation which in turn promotes phonon scattering and thus a lower lattice thermal

conductivity. These characteristics result in very low thermal conductivity materials, a desirable feature for achieving high-performance thermoelectric materials.

The figure of merit of $Rb_{0.2}Ba_{0.4}Cr_5Se_8$ was evaluated to determine its thermoelectric efficiency (**Figure 10**). Values rise from about 0.05 at 300 K to a peak value of 0.22 at 873 K. In particular, its figure of merit exhibits substantially larger values than $Ba_{0.5}Cr_5Se_8$ on the entire temperature range. This enhancement is attributed to an enhanced power factor due to synergistic effects on the electrical transport properties and a slightly lower thermal conductivity resulting from the presence of both Rb and Ba cations inside the channels. Although its performance falls short of that of $Tl_xCr_5Se_8$, primarily due to the high level of degeneracy leading to a low resistivity in the latter compound, $Rb_{0.2}Ba_{0.4}Cr_5Se_8$ presents a notably higher thermopower. These findings suggest promising avenues for future thermoelectric optimizations within the double-inserted pseudo-hollandite family of compounds.

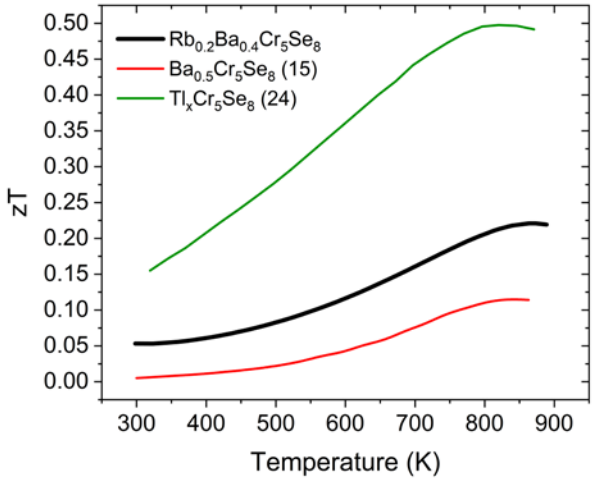

Figure 10. Evolution of the thermoelectric figure of merit of $Rb_{0.2}Ba_{0.4}Cr_5Se_8$ (black) and comparison with other pseudo-hollandite compounds ($Ba_{0.5}Cr_5Se_8$ in red and $Tl_xCr_5Se_8$ in green).

CONCLUSION

In this study, a novel quaternary pseudo-hollandite $Rb_{0.2}Ba_{0.4}Cr_5Se_8$ was successfully synthesized and characterized to elucidate its structural and transport properties. Single crystals were grown, and detailed single-crystal X-ray diffraction analysis revealed a one-dimensional structure with mixed occupancy of Rb and Ba atoms within the channels. The observed anisotropic atomic displacement parameters were attributed to atomic disorder on the cationic site 2*a* in the space group *C*2/*m*. Polycrystalline samples were synthesized and confirmed as single phase by powder X-ray diffraction. High-temperature X-ray diffraction patterns indicated the compound's thermal stability without decomposing into secondary phases. The thermal expansion coefficient, a critical factor for device implementation, was determined to be $2.6(1) \times 10^{-5}$ K^{-1} at 300 K, representing to the best of our knowledge the first reported value in hollandite derivatives. A theoretical investigation unveiled the density of states distribution and Seebeck coefficient of both $Rb_{0.2}Ba_{0.4}Cr_5Se_8$ and $Ba_{0.5}Cr_5Se_8$, providing insights into the transport properties of both compounds. Resistivity measurements of the title compound demonstrated an intermediate electrical conductive mode, in particular a partially degenerate semiconducting behavior from 300 to 873 K. Thermal conductivity measurements indicated values below 1 $W.m^{-1}.K^{-1}$, slightly lower than $Ba_{0.5}Cr_5Se_8$ but higher than $Tl_xCr_5Se_8$. Conversely, the Seebeck coefficient is consistently higher, reaching a maximum of 400 $\mu V.K^{-1}$ at 620 K. The decorrelated transport properties induced by an increased hole effective mass contribute to a larger figure of merit for $Rb_{0.2}Ba_{0.4}Cr_5Se_8$ compared to that of $Ba_{0.5}Cr_5Se_8$, with a maximum value of 0.22 at 673 K, surpassing that of $Ba_{0.5}Cr_5Se_8$ (0.12 at 835 K). While $Tl_xCr_5Se_8$ remains the most efficient thermoelectric material in this family of compounds, the toxicity of thallium makes $Rb_{0.2}Ba_{0.4}Cr_5Se_8$ a decent alternative. Overall, this study highlights the potential of double-inserted pseudo-hollandites as promising candidates for achieving high-performance thermoelectric materials.

ASSOCIATED CONTENT

Supporting Information

The Supporting Information (Crystallographic Information File) is available free of charge at https://pubs.acs.org/

AUTHOR INFORMATION

Corresponding Authors

Hugo Bouteiller – orcid.org/0009-0004-2132-2962; Email: hugo.bouteiller@univ-poitiers.fr

Jean-François Halet – orcid.org/0000-0002-2315-4200; Email: jean-francois.halet@univ-rennes.fr

David Berthebaud – orcid.org/0000-0002-2892-2125; Email: david.berthebaud@cnrs.fr

Authors

Bruno Fontaine – Email: bruno.fontaine@ensc-rennes.fr

Olivier Perez – Email: olivier.perez@ensicaen.fr

Sylvie Hébert – orcid.org/0000-0001-7412-2367; Email: sylvie.hebert@ensicaen.fr

Cédric Bourgès – orcid.org/0000-0001-9056-0420; Email: bourges.cedric@nims.go.jp

Yoshitaka Matsushita – orcid.org/ 0000-0002-4968-8905; Email: matsushita.yoshitaka@nims.go.jp

Takao Mori – orcid.org/0000-0003-2682-1846; Email: mori.takao@nims.go.jp

Franck Gascoin – orcid.org/0000-0002-9791-1358; Email: franck.gascoin@ensicaen.fr

Author Contributions

HB: conceptualization, data curation, formal analysis, investigation, methodology, validation, visualization, writing – original draft, writing – review & editing. **BF**: software, data curation, formal analysis, investigation, validation. **OP**: data curation, formal analysis, validation, writing – review & editing. **SH**: data curation, formal analysis, validation, writing – review & editing. **CB**: data curation, formal analysis, validation, writing – review & editing. **YM**: data curation, formal analysis, validation, writing – review & editing. **TM**: funding acquisition, resources, supervision, writing – review & editing. **FG**: conceptualization, funding acquisition, validation, project

administration, resources, supervision. **J-FH**: conceptualization, software, data curation, formal analysis, investigation, visualization, validation, supervision, writing – review & editing. **DB**: conceptualization, formal analysis, investigation, methodology, visualization, project administration, resources, supervision, writing – review & editing.

ACKNOWLEDGMENTS

The authors are grateful to the Agence Nationale de la Recherche (ANR – Project HIGHTHERM – Ref ANR-18-CE05-0037) and the Japan Society for the Promotion of Science (JSPS – PE21708 and 19H05819) for financial support. Support from JST Mirai Program JPMJMI19A1 is also acknowledged.

Notes

The authors declare no competing financial interest.

REFERENCES

(1) Salarizadeh, P.; Rastgoo-Deylami, M.; Askari, M. B.; hooshyari, K. A Short Review on Transition Metal Chalcogenides/Carbon Nanocomposites for Energy Storage. *Nano Futur.* **2022**, *6* (3), 032005.

(2) Dai, M.; Wang, R. Synthesis and Applications of Nanostructured Hollow Transition Metal Chalcogenides. *Small* **2021**, *17* (29), 2006813.

(3) Huang, Y. L.; Chen, W.; Wee, A. T. S. Two-Dimensional Magnetic Transition Metal Chalcogenides. *SmartMat* **2021**, *2* (2), 139–153.

(4) Lu, H.-L.; Zhang, Y.-Y.; Lin, X.; Gao, H.-J. Novel Two-Dimensional Transition Metal Chalcogenides Created by Epitaxial Growth. *Sci. China Phys. Mech. Astron.* **2021**, *64* (10), 106801.

(5) Zhu, S.-C.; Xiao, F.-X. Transition Metal Chalcogenides Quantum Dots: Emerging Building Blocks toward Solar-to-Hydrogen Conversion. *ACS Catal.* **2023**, *13* (11), 7269–7309.

(6) Romanenko, A. I.; Chebanova, G. E.; Chen, T.; Su, W.; Wang, H. Review of the Thermoelectric Properties of Layered Oxides and Chalcogenides. *J. Phys. Appl. Phys.* **2021**, *55* (14), 143001.

(7) Hébert, S.; Daou, R.; Maignan, A.; Das, S.; Banerjee, A.; Klein, Y.; Bourgès, C.; Tsujii, N.; Mori, T. Thermoelectric Materials Taking Advantage of Spin Entropy: Lessons from Chalcogenides and Oxides. *Sci. Technol. Adv. Mater.* **2021**, *22* (1), 583–596.

(8) McKeever, H.; Patil, N. N.; Palabathuni, M.; Singh, S. Functional Alkali Metal-Based Ternary Chalcogenides: Design, Properties, and Opportunities. *Chem. Mater.* **2023**, *35* (23), 9833–9846.

(9) Snyder, G. J.; Toberer, E. S. Complex Thermoelectric Materials. *Nat. Mater.* **2008**, *7* (2), 105–114.

(10) Dresselhaus, M. S.; Chen, G.; Tang, M. Y.; Yang, R.; Lee, H.; Wang, D.; Ren, Z.; Fleurial, J. P.; Gogna, P. New Directions for Low-Dimensional Thermoelectric Materials. *Adv. Mater.* **2007**, *19* (8), 1043–1053.

(11) Kauzlarich, S. M.; Devlin, K. P.; Perez, C. J. Zintl Phases for Thermoelectric Applications. *Thermoelectr. Energy Convers. Theor. Mech. Mater. Devices Appl.* **2021**, 157–182.

(12) Chen, X.; Zhou, Z.; Lin, Y. H.; Nan, C. Thermoelectric Thin Films: Promising Strategies and Related Mechanism on Boosting Energy Conversion Performance. *J. Materiomics* **2020**, *6* (3), 494–512.

(13) Dehkordi, A. M.; Zebarjadi, M.; He, J.; Tritt, T. M. Thermoelectric Power Factor: Enhancement Mechanisms and Strategies for Higher Performance Thermoelectric Materials. **2015**.

(14) Hendricks, T.; Caillat, T.; Mori, T. Keynote Review of Latest Advances in Thermoelectric Generation Materials, Devices, and Technologies 2022. *Energies.* **2022**, *15* (19), 7307.

(15) Lefèvre, R.; Berthebaud, D.; Perez, O.; Pelloquin, D.; Hébert, S.; Gascoin, F. Polar Transition-Metal Chalcogenide: Structure and Properties of the New Pseudo-Hollandite $Ba_{0.5}Cr_5Se_8$. *Chem. Mater.* **2015**, *27* (20), 7110–7118.

(16) Ohtani, T.; Onoue, S. Preparation and Magnetic Properties of the New Ternary Chalcogenides Isotypic with TlV_5S_8 and TlV_6S_8. *Mater. Res. Bull.* **1986**, *21* (1), 69–76.

(17) Ohtani, T.; Sano, Y.; Kodama, K.; Onoue, S.; Nishihara, H. Synthesis of New Ternary Tunnel Chalcogenides by Ion Exchange Reactions and Deintercalation of the Ternary Chromium Selenides. *Mater. Res. Bull.* **1993**, *28* (5), 501–508.

(18) Yamazaki, S.; Ueda, Y. New Ferromagnetic Chromium Chalcogenides, ACr_5Te_8 (A = K, Cs and Rb). *Solid State Phenom.* **2011**, *170*, 17–20.

(19) Gareh, J.; Boucher, F.; Evain, M.; O'Connor, C. J.; Li, S. Synthesis and Crystal Structure of the New Hollandite-like Channel Phase $Rb_{0.73}Cr_5Te_8$. *J. Solid State Chem.* **1996**, *122* (1), 41–45.

(20) Boucher, F.; Gareh, J.; Gourdon, O.; Evain, M.; O'Connor, C. J. Synthesis and Crystal Structure of the Pseudo-Hollandite $Rb_{0.62}Cr_5Te_8$ and Analysis of the Electronic Band Structures of the $Rb_xCr_5Te_8$ Phases. *J. Solid State Chem.* **1997**, *131* (2), 326–334.

(21) Bensch, W.; Sander, B.; Helmer, O.; Näther, C.; Tuczek, F.; Shames, A. I.; Panich, A. M. Evidences for the Formation of Chromium in the Unusual Oxidation State Cr(IV): II. Magnetic Properties and Low-Temperature X-Ray Investigations of the Nonstoichiometric Channel Compounds $Tl_xCr_5Se_8$ ($0 \leq x \leq 1$). *J. Solid State Chem.* **1999**, *145* (1), 235–246.

(22) Saßmannshausen, M.; Lutz, H. D. Thermal Motion of the Univalent Metal Ions in KCr_5S_8-Type Chalcogenides, Ternary Chromium Selenides $M_xCr_5Se_8$ (M = Rb, Cs). *Z. Krist.* **2000**, *215* (36831), 683.

(23) Hébert, S.; Berthebaud, D.; Daou, R.; Bréard, Y.; Pelloquin, D.; Guilmeau, E.; Gascoin, F.; Lebedev, O.; Maignan, A. Searching for New Thermoelectric Materials: Some Examples among Oxides, Sulfides and Selenides. *J. Phys. Condens. Matter* **2015**, *28* (1), 013001.

(24) Takahashi, H.; Raghavendra, N.; Gascoin, F.; Pelloquin, D.; Hébert, S.; Guilmeau, E. Transport Properties of an Intermetallic with Pseudo-Hollandite Structure as a Potential Thermoelectric Material: The Example of $Tl_xCr_5Se_8$. *Chem. Mater.* **2013**, *25* (9), 1809–1815.

(25) Lefèvre, R.; Berthebaud, D.; Bux, S.; Hébert, S.; Gascoin, F. Magnetic and Thermoelectric Properties of the Ternary Pseudo-Hollandite $Ba_xCr_5Se_8$ ($0.5 < x < 0.55$) Solid Solution. *Dalton Trans.* **2016**, *45* (30), 12119–12126.

(26) Maier, S.; Lefèvre, R.; Lin, X.; Nunna, R.; Berthebaud, D.; Hèbert, S.; Mar, A.; Gascoin, F. The Solid Solution Series $Tl(V_{1-x}Cr_x)_5Se_8$: Crystal Structure, Magnetic and Thermoelectric Properties. *J. Mater. Chem. C* **2015**, *3* (40), 10509–10517.

(27) Huster, J. Darstellung Und Kristallstruktur Der Alkalithiochromate (III), ACr_5S_8 (A ≙ Cs, Rb Und K). *Z. Anorg. Allg. Chem.* **1978**, *447* (1), 89–96.

(28) Klepp, K.; Boller, H. Channel Structures Based on Octahedral Frameworks: The Crystal Structure of $TlTi_5Se_8$, TlV_5Se_8, and $TlCr_5Se_8$ and Its Relationships to $TlCr_3S_5$, Hollandites, and Psilomelane. *J. Solid State Chem.* **1983**, *48* (3), 388–395.

(29) Bronsema, K. D.; Jansen, R.; Wiegers, G. A. The Preparation, Crystal Structures and Properties of the Potassium Vanadium Sulfides $K_xV_5S_8$ ($0.5 \leqq x \leqq 0.7$). *Mater. Res. Bull.* **1984**, *19* (5), 555–562.

(30) Bronger, W.; Herudek, C.; Huster, J.; Schmitz, D. New Alkali Metal Chromium Chalcogenides and Their Structural Classification. *Z. Für Anorg. Allg. Chem.* **1993**, *619* (2), 243–252.

(31) Novet, T.; Wagner, M.; Jiang, M.; Johnson, D. C. The Preparation and Properties of $M'M_5X_8$ (X = Se, Te; M = Cr, Ti; M' = Li, Na, K, Rb, Cs, Cd, Sn, Pb) via Low Temperature Ion Exchange Reaction. *Mater. Res. Bull.* **1995**, *30* (1), 65–73.

(32) Ohtani, T.; Onoue, S. The Phase Study of the Tl-V-S System and the Properties of TlV_6S_8 and TlV_5S_8 Phases. *J. Solid State Chem.* **1985**, *59* (3), 324–331.

(33) Schramm, W.; Schöllhorn, R.; Eckert, H.; Müller-Warmuth, W. Nonstoichiometric Channel Chalcogenides $Tl_xV_5S_8$: Topotactic Redox Reactions and NMR Studies. *Mater. Res. Bull.* **1983**, *18* (10), 1283–1289.

(34) Quint, R.; Boller, H. On the Crystal Chemistry of Hollandite-like Phases with TlV_5S_8 Structure: The Crystal Structures of $Tl_xTi_5S_8$, $Tl_xV_5S_8$ and $TlCr_5S_8$. *Mater. Res. Bull.* **1987**, *22* (11), 1499–1504.

(35) Fournès, L.; Vlasse, M.; Saux, M. Preparation, Properties and Crystal Structure of TlV_5S_8. *Mater. Res. Bull.* **1977**, *12* (1), 1–5.

(36) Boller, H.; Klepp, K. O.; Kirchmayr, K. On the Knowledge of Two Thallium-Tellurochromites [$TlCrTe_2$ and $TlCr_5Te_8$]. *Mater. Res. Bull.* **1995**, *30* (3), 365–371.

(37) Yamazaki, S.; Ueda, Y. Synthesis, Structures and Magnetic Properties of Pseudo-Hollandite Chromium Sulfides. *J. Solid State Chem.* **2010**, *183* (9), 1905–1911.

(38) Lefevre, R.; Berthebaud, D.; Gascoin, F. Substitution of Indium for Chromium in $TlIn_{5-x}Cr_xSe_8$: Crystal Structure of $TlIn_{4.811(5)}Cr_{0.189(5)}Se_8$. *Acta Crystallogr. Sect. E Crystallogr. Commun.* **2017**, *73* (Pt 4), 500–502.

(39) Bensch, W.; Sander, B. The Influence of Sulfur and Selenium onto the Physicochemical Properties of the Quasi-Ternary Chromium Chalcogenides $TlCr_5S_{8-z}Se_z$ (z = 0–8). *Solid State Sci.* **2002**, *4* (5), 701–708.

(40) Gray, D. L.; Ibers, J. A. Synthesis and Structure of $CsTi_5Te_8$: Relation to the TlV_5S_8, $TlCr_3S_5$, and Similar Channel Structures. *J. Alloys Compd.* **2007**, *440* (1–2), 74–77.

(41) Babo, J.-M.; Schleid, T. Synthesis and Crystal Structure of the Rubidium Scandium Telluride $RbSc_5Te_8$. *Z. Für Anorg. Allg. Chem.* **2008**, *634* (9), 1463–1465.

(42) Bouteiller, H.; Fontaine, B.; Mori, T.; Gascoin, F.; Halet, J.-F.; Berthebaud, D. Synthesis, Crystal and Electronic Structure, and Thermal Conductivity Investigation of the Hollandite-like $Cs_xCr_5Te_8$ Phases ($0.73 < x < 1$). *Inorg. Chem.* **2023**, *62* (41), 16905–16912.

(43) Oxford Diffraction - Agilent Technologies UK Ltd. CrysAlis PRO, 2014.

(44) Palatinus, L.; Chapuis, G. SUPERFLIP - A Computer Program for the Solution of Crystal Structures by Charge Flipping in Arbitrary Dimensions. *J. Appl. Crystallogr.* **2007**, *40* (4), 786–790.

(45) Petrícek, V.; Dušek, M.; Palatinus, L. Crystallographic Computing System JANA2006: General Features. *Z. Krist.* **2014**, *229* (5), 345–352.

(46) Rodriguez-Carvajal, J. Fullprof: A Program for Rietveld Refinement and Pattern Matching Analysis. *Abstr. Satell. Meet. Powder Diffr. XV Congr. IUCr* **1990**, 127.

(47) Kresse, G.; Hafner, J. Ab Initio Molecular Dynamics for Liquid Metals. *Phys. Rev. B* **1993**, *47* (1), 558-561.

(48) Kresse, G.; Furthmüller, J. Efficient Iterative Schemes for Ab Initio Total-Energy Calculations Using a Plane-Wave Basis Set. *Phys. Rev. B* **1996**, *54* (16), 11169-11186.

(49) Kresse, G.; Furthmüller, J. Efficiency of Ab-Initio Total Energy Calculations for Metals and Semiconductors Using a Plane-Wave Basis Set. *Comput. Mater. Sci.* **1996**, *6* (1), 15–50.

(50) Perdew, J. P.; Burke, K.; Ernzerhof, M. Generalized Gradient Approximation Made Simple. *Phys. Rev. Lett.* **1996**, *77* (18), 3865–3868.

(51) Monkhorst, H. J.; Pack, J. D. Special Points for Brillouin-Zone Integrations. *Phys. Rev. B* **1976**, *13* (12), 5188–5192.

(52) Blaha, P.; Schwarz, K.; Tran, F.; Laskowski, R.; Madsen, G. K. H.; Marks, L. D. WIEN2k: An APW+lo Program for Calculating the Properties of Solids. *J. Chem. Phys.* **2020**, *152* (7), 074101.

(53) Tran, F.; Blaha, P. Accurate Band Gaps of Semiconductors and Insulators with a Semilocal Exchange-Correlation Potential. *Phys. Rev. Lett.* **2009**, *102* (22), 226401.

(54) Madsen, G. K. H.; Carrete, J.; Verstraete, M. J. BoltzTraP2, a Program for Interpolating Band Structures and Calculating Semi-Classical Transport Coefficients. *Comput. Phys. Commun.* **2018**, *231*, 140–145.

(55) Scheidemantel, T. J.; Ambrosch-Draxl, C.; Thonhauser, T.; Badding, J. V.; Sofo, J. O. Transport Coefficients from First-Principles Calculations. *Phys. Rev. B* **2003**, *68* (12), 125210.

(56) Madsen, G. K. H. Automated Search for New Thermoelectric Materials: The Case of LiZnSb. *J. Am. Chem. Soc.* **2006**, *128* (37), 12140–12146.

(57) *Advanced Thermoelectrics: Materials, Contacts, Devices, and Systems*. Ren, Z.; Lan, Y.; Zhang, Q., Eds.; CRC Press: Boca Raton, **2017**.

(58) Gurukrishna, K.; Nikhita, H. R.; Swamy, S. M. M.; Rao, A. Existence of Partially Degenerate Electrical Transport in Intermetallic Cu_2SnSe_3 Thermoelectric System Sintered at Different Temperatures. *Met. Mater. Int.* **2022**, *28* (8), 2023–2032.

(59) *CRC Handbook of Thermoelectrics*. Rowe, D. M., Ed.; CRC Press: Boca Raton, **1995**.

(60) Li, X. Y.; Li, D.; Xin, H. X.; Zhang, J.; Song, C. J.; Qin, X. Y. Effects of Bismuth Doping on the Thermoelectric Properties of Cu_3SbSe_4 at Moderate Temperatures. *J. Alloys Compd.* **2013**, *561*, 105–108.

(61) Li, J. M.; Li, D.; Song, C. J.; Wang, L.; Xin, H. X.; Zhang, J.; Qin, X. Y. Realized High Power Factor and Thermoelectric Performance in Cu_3SbSe_4. *Intermetallics* **2019**, *109*, 68–73.

For Table of Contents Only

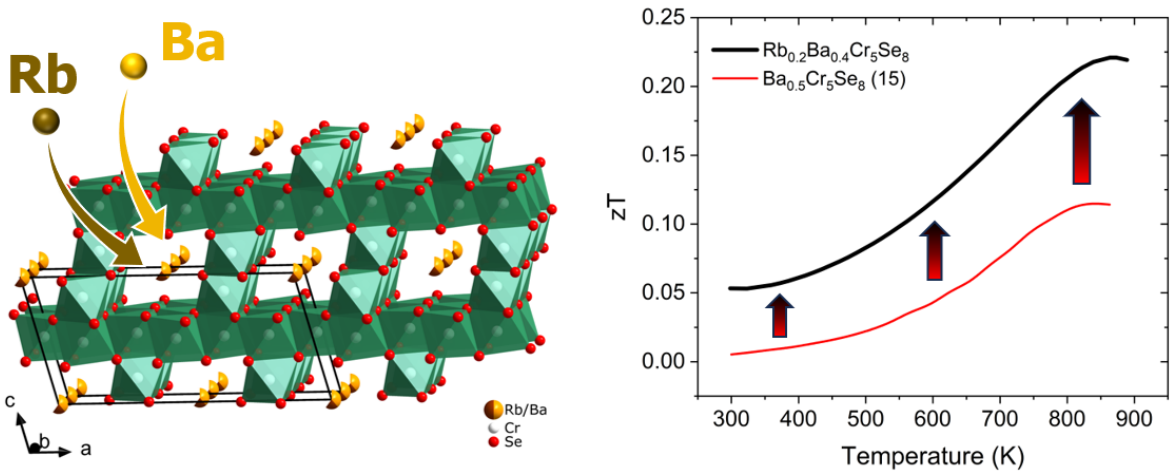

Synopsis:

A novel quaternary pseudo-hollandite $Rb_{0.2}Ba_{0.4}Cr_5Se_8$ inserted with both Rb and Ba in the quasi-one-dimensional channel structure was synthesized and characterized in this study. A decorrelation of the transport properties was observed, leading to a significant improvement of the thermoelectric properties in this compound.